The 6th International Symposium – Supercritical CO_2 Power Cycles
March 27-29, 2018, Pittsburgh, Pennsylvania

Dynamic Modeling of Microtube Recuperators in an Indirect Supercritical Carbon Dioxide Recompression Closed Brayton Power Cycle

Yuan Jiang [a], Eric Liese [a*], Stephen E. Zitney [a,b], Debangsu Bhattacharyya [b]

a) National Energy Technology Laboratory, 3610 Collins Ferry Rd, Morgantown, WV 26507, USA
b) Dept. of Chemical and Biomedical Eng., West Virginia University, Morgantown, WV 26506, USA

ABSTRACT

In this study, a dynamic model of a microtube shell-and-tube heat exchanger has been developed in Aspen Custom Modeler (ACM) for a high temperature (HT) and low temperature (LT) recuperator in a 10 MWe indirect supercritical carbon dioxide (sCO_2) recompression closed Brayton cycle (RCBC) power plant. This model can be easily implemented into the plant-wide dynamic model developed in Aspen Plus Dynamic to investigate the system dynamic behavior, start-up, shut-down and control strategies of the proposed novel sCO_2 RCBC plant. The operating conditions of the recuperators are determined by a system-level analysis, while the recuperators' geometry is optimized by a previously developed steady-state design model. In this dynamic model, only axial temperature variations are considered for the hot and cold fluids as well as the metal walls when computing heat, mass and momentum balances. The heat transfer coefficients and friction factors are calculated using empirical equations proven for sCO_2 fluids. Sensitivity studies have been conducted to analyze the effect of the discretization size and the time integral step size. Step changes and different ramp rates have been introduced to both HT and LT recuperators to test the dynamic behavior and numerical robustness. The results indicate that for the conditions studied here, the shell wall heat conduction has negligible effect on the steady-state and transient thermal performance of the recuperators, and the dynamic responses of the proposed compact recuperators are fast due to the small Biot number, metal mass and high heat transfer coefficient of the microtube shell-and-tube heat exchangers. These fast dynamic responses are consistent with the small lumped thermal residence time reported by a previously developed steady-state optimal design model.

Key Words

Supercritical CO_2, Power Cycle, Microtube Recuperator, Dynamic Modeling, Aspen Customer Modeler

---

[*] Eric Liese, National Energy Technology Laboratory, 3610 Collins Ferry Rd, Morgantown, WV 26507
Tel: +1(304)285-4610, E-mail: Eric.Liese@netl.doe.gov

1. Introduction

The supercritical carbon dioxide (sCO_2) power cycle is a promising technology due to its potential higher efficiency and smaller turbomachinery compared with steam cycles (Zitney and Liese, 2016). Different from typical steam cycles, the whole sCO_2 RCBC plant is usually operated above the critical point of CO_2, and therefore undergoes drastic density changes instead of phase change over the operating range of temperature and pressure (Ahn et al., 2015). Thus, the engineering and operating experience as well as modeling approach of the conventional steam cycles cannot be directly applied to the sCO_2 power cycle. In the sCO_2 recompression closed Brayton cycle (RCBC) plant, the turbine outlet temperature is still high due to the small pressure ratio (Zitney and Liese, 2016). A considerable amount of energy has to be recovered by exchanging heat between hot turbine outlet stream and the cold inlet stream in order to achieve higher overall cycle efficiency (Jiang et al., 2017). Specially designed compact heat exchangers are superior to the conventional shell-and-tube heat exchanger in terms of capital cost and footprint (Jiang et al., 2017). Customized models are required since most of the conventional design and rating models are developed based on a constant property assumption, which is clearly not practical in sCO_2 cycles (Xie et al., 2008; Guo, 2016). Hence, the design and modeling of recuperators is of crucial importance.

Among different types of compact heat exchangers, microtube and printed circuit heat exchangers have been recommended for sCO_2 power cycles based on the experience of multiple researchers (Musgrove et al., 2017; Carstens, 2007; Chordia et al., 2016; Luu et al., 2017). In the sCO_2 RCBC test article built by Sandia National Laboratory, printed circuit heat exchangers were one of the selections (Kruizenga et al., 2014). Schmitt et al. designed micro-channel recuperators for a 100 MWe sCO_2 RCBC plant, of which the geometry is similar to that of microtube exchanger (Schmitt et al., 2015). Chordia et al. conducted preliminary designs for multiple types of heat exchangers, including microtube, stacked-sheet, plate-fin, double-pipe, etc., and suggested microtube heat exchanger for the 10 MWe sCO_2 RCBC plant (Chordia et al., 2016). The microtube shell-and-tube heat exchanger is like the conventional shell-and-tube heat exchanger, but using smaller tube diameters on the order of 1 mm instead of baffles in the shell to provide larger heat transfer coefficient to both shell and tube sides (Jiang et al., 2017; Musgrove et al., 2017). Previously, the National Energy Technology Laboratory (NETL) has developed an optimal design model of microtube shell-and-tube recuperators for sCO_2 RCBC application (Jiang et al., 2017). In this design model, the recuperator geometry variables are optimized in Aspen Custom Modeler (ACM) using a successive quadratic programming method with rigorous energy balance constraints, geometry calculations, and thermal-hydraulic correlations proven for sCO_2 flow (Jiang et al., 2017).

It is noted that the existing rigorous simulation studies of heat exchangers in thermal systems, especially the sCO_2 based power cycle, are mostly steady-state analysis for system design and optimization (Guo, 2016; Xie et al., 2008; Schmitt et al., 2015). Few system-level dynamic studies are conducted based on rigorous non-conventional equipment models specialized for the application in sCO_2 power cycles (Zitney and Liese, 2016; Carstens, 2007; Luu et al., 2017; Francesco and Piero, 2011; Carstens, 2007). Since a reasonable estimation of dynamic behaviors of each component is critical when investigating the start-up, shut-down and load-following control strategies of the novel sCO_2 RCBC plant, in this study we developed a one-dimensional (1D) dynamic model for the microtube recuperators in a 10 MWe sCO_2 RCBC plant – with a turbine inlet temperature of 700°C and mass flow rate of ~ 100 kg/s - using the geometry design optimized by the design model developed by NETL previously. The paper presents the modeling approach and comparison, discretization sensitivity analysis, as well as the dynamic behaviors of the microtube recuperators subjected to changing inlet temperature and flowrate.

2. Dynamic model

In this study, microtube shell-and-tube heat exchangers are used to recuperate heat in the sCO_2 RCBC (Zitney and Liese, 2016; Jiang et al., 2017), which is similar to conventional shell-and-tube exchangers but with smaller tube size and considering no baffle in the shell (Musgrove et al., 2017). In the recuperator, the fluids flow counter-currently, where the cold high-pressure sCO_2 stream enters the tube side. A detailed optimal design model has been developed in a previous NETL study considering an industrial standard tube size (Jiang et al., 2017). The key design parameters are the number of tubes (N_t), tube

diameter (D_{to}), pitch layout, and pitch to diameter ratio (P_t/D_{to}), where pitch is the distance between tube centerlines. The tube length (L) and shell diameter (D_{so}) can be evaluated based on the above design parameters and the desired extent of heat recovery (Jiang et al., 2017). The minimum thickness of tube wall, and the thickness of shell wall and tube sheet are calculated using ASME and TEMA standards. For the 10 MWe plant, the stream conditions and heat duty of the high temperature (HT) and low temperature (LT) recuperators are determined by the system-level model as shown in Table 1 (Zitney and Liese, 2016). The heat duty for the HT recuperator is 45.2 MWt, and the LT recuperator is 14.5 MWt. The general geometry variables as shown in Table 2 are given by the steady-state optimization model considering standard SS 316 microtubes (Jiang et al., 2017).

Table 1 Operating conditions of the recuperators in the 10 MWe sCO_2 cycle

	HT	LT		HT	LT
$T_{h,in}$ (°C)	578.15	191.95	$T_{h,out}$ (°C)	191.95	78.55
$T_{c,in}$ (°C)	181.95	68.20	$T_{c,out}$ (°C)	531.35	181.95
$P_{h,in}$ (bar)	89.62	86.87	$P_{h,out}$ (bar)	86.87	85.37
$P_{c,in}$ (bar)	237.48	238.69	$P_{c,out}$ (bar)	237.48	238.51
F_h (kg/s)	100.17	100.17	F_c (kg/s)	100.17	64.51

Table 2 Optimal design of recuperators in the 10 MWe sCO_2 cycle

	HT recuperator	LT recuperator
Number of tube, N_t	47174	62872
Pitch layout	Triangular	Triangular
Pitch ratio, P_t/D_{to}	1.25	1.257
Tube outer diameter, D_{to} (mm)	2.381	1.586
Tube thickness, t (mm)	0.406	0.330
Tube length, L (m)	3.651	2.263

Transient heat, momentum and mass balance equations are developed for the hot and cold fluid in Aspen Custom Modeler (ACM). The NETL system dynamic model of the 10 MW RCBC cycle uses AspenTech® software, and ACM is a higher-level language modeling software tool for building non-library models. Heat conduction in the tube and shell wall is also considered. The ACM model is developed based on the following assumptions: (1) fully developed turbulent flow in both tube and shell sides, (2) ideal counter-current and annulus flow along tubes in the shell side, (3) negligible axial dispersion effects, (4) negligible radial temperature distribution in the hot fluid, cold fluid, and wall, (5) negligible heat losses to the environment, (6) quasi-static assumptions for evaluating the friction factor and the heat transfer coefficients (Carstens, 2007; Vaitekunas, 1990).

2.1 Heat balance

With the above assumptions, the 1D transient forced convection heat transfer equation of the cold sCO_2 flow in the tube side can be written as Eq. (1), with the boundary condition given by Eq. (2).

$$\left(\frac{\pi}{4}N_t D_{ti}^2\right)\frac{\partial(\rho_c U_c)}{\partial t} = -\frac{\partial(G_c H_c)}{\partial z} + h_c(\pi N_t D_{ti})\,(T_t - T_c) \tag{1}$$

$$(T_c)_{z=0} = T_{c,in} \tag{2}$$

Usually, heat conduction in the shell wall is negligible due to the large heat conductivity and small metal mass (Simoes et al., 2005). If the heat conduction in the shell wall is not considered, the heat balance of the hot sCO_2 flow in the shell side can be written as Eq. (3), with the boundary condition given by Eq. (4).

$$\frac{\pi}{4}(D_{si}^2 - N_t D_{to}^2)\frac{\partial(\rho_h U_h)}{\partial t} = \frac{\partial(G_h H_h)}{\partial z} + h_h(\pi N_t D_{to})\,(T_t - T_h) \tag{3}$$

$$(T_h)_{z=L} = T_{h,in} \tag{4}$$

In Eqs. (1) and (3), symbols ρ, U, H, G, h, and T denote the density, molar internal energy, molar enthalpy, molar flowrate, convection heat transfer coefficient, and temperature of the cold (c) and hot (h) sCO_2 fluids, respectively. D_{ti}, D_{to} and D_{si} are the tube inner and outer diameter, and the shell inner diameter, respectively. T_t is the tube wall temperature given by the 1D heat conduction equation as shown in Eq. (5) with the boundary condition given by Eq. (6). In Eq. (5), symbols ρ_t, C_{pt}, and k_t denote the density, specific heat and heat conductivity of the tube wall, respectively. Here, the heat conduction in the radial direction is neglected because of its small Biot number (Bi<0.1).

$$\rho_t C_{pt}\frac{\partial T_t}{\partial t} = k_t\frac{\partial^2 T_t}{\partial z^2} + \frac{4h_h D_{to}(T_h - T_t)}{D_{to}^2 - D_{ti}^2} - \frac{4h_c D_{ti}(T_t - T_c)}{D_{to}^2 - D_{ti}^2} \tag{5}$$

$$\left(\frac{\partial T_t}{\partial z}\right)_{z=0} = \left(\frac{\partial T_t}{\partial z}\right)_{z=L} = 0 \tag{6}$$

If the heat conduction in the shell wall is considered, the heat transfer between the hot fluid and the shell wall must be considered as well. The new transient heat balance of the hot fluid can be written as Eq. (7) by including the heat flux between the hot fluid and the shell wall into Eq. (3). In Eq. (7), h_h' is the convection heat transfer coefficient between the hot fluid and shell wall.

$$\frac{\pi}{4}(D_{si}^2 - N_t D_{to}^2)\frac{\partial(\rho_h U_h)}{\partial t} = \frac{\partial(G_h H_h)}{\partial z} + h_h(N_t\pi D_{to})(T_t - T_h) + h_h'(\pi D_{si})(T_s - T_h) \tag{7}$$

Similarly, the Biot number of the shell wall is smaller than 0.1, and thus the heat conduction in the radial direction can be neglected. The 1D heat conduction in the shell wall can be written as Eq. (8), with the boundary condition given by Eq. (9), where D_{so}, ρ_s, C_{ps}, and k_s are the shell outer diameter, density, specific heat and heat conductivity, respectively.

$$\rho_s C_{ps}\frac{\partial T_s}{\partial t} = k_s\frac{\partial^2 T_s}{\partial z^2} + \frac{4h_h' D_{si}(T_h - T_s)}{D_{so}^2 - D_{si}^2} \tag{8}$$

$$\left(\frac{\partial T_s}{\partial z}\right)_{z=0} = \left(\frac{\partial T_s}{\partial z}\right)_{z=L} = 0 \tag{9}$$

2.2 Mass and momentum balance

The mass and momentum balance of the hot and cold sCO_2 fluids are given by Eqs. (10) and (11), where v, f, D_{hd}, and P denote the velocity, Darcy friction factor, hydraulic diameter and pressure of the hot or cold sides, respectively. The inlet pressure and velocity are given as the boundary conditions.

$$\frac{\partial \rho}{\partial t} + \frac{\partial(\rho v)}{\partial z} = 0 \tag{10}$$

$$\frac{\partial(\rho v)}{\partial t} = -\frac{\partial(\rho v v)}{\partial z} - \frac{dP}{dz} \pm \frac{1}{2}\rho v^2 f / D_{hd} \tag{11}$$

2.3 Property model and thermal-hydraulic correlations

In this study, REFPROP is used to evaluate the properties of sCO_2 fluids (Jiang et al., 2017; Span and Wagner, 1996). The $k - T$ correlation and $C_p - T$ correlation of the tube and shell wall are available in the open literatures for SS316 (Jiang et al., 2017). The thermal-hydraulic performance of the recuperators are characterized by the modified Dittus-Boelter equation (Eq. (12)) and Colebrook–White equation (Eqs. (13) and (14)) with wall temperature correction terms, which have been proven for sCO_2 flow in microtubes (Musgrove, 2017; Jackson, 2013, Jiang et al., 2017). Here, ρ_w is the fluid density evaluated at tube wall temperature ($T_w = T_t$) and fluid pressure. In Eq. (13), the relative tube roughness (ε/D) is assumed to be 0.0005. D_{hd} is the hydraulic diameter used for pressure drop calculation, D_{ti} for the tube side, D'_{se} defined in Eq. (19) for the shell side.

$$Nu = 0.023 Re^{0.8} Pr^{0.5} \left(\frac{\rho_w}{\rho}\right)^{0.3} \tag{12}$$

$$\frac{1}{\sqrt{f_{cp}}} = -2log\left(\frac{\varepsilon}{3.7 D_{hd}} + \frac{2.51}{Re\sqrt{f_{cp}}}\right) \tag{13}$$

$$\frac{f}{f_{cp}} = \left(\frac{T}{T_w}\right)^{0.1} \tag{14}$$

The hydraulic diameters of the tube side and the shell side are different, and furthermore, they are also different when evaluating heat transfer (Nusselt number) and pressure drop (Reynolds number) (Jiang et al., 2017). Eqs. (15) to (17) provide more detailed equations for evaluating the three heat transfer coefficients h_c, h_h, and h'_h in the heat balance equations discussed in Section 2.1.

$$\frac{h_c D_{ti}}{k_c} = 0.023 \left(\frac{\rho_c v_c D_{ti}}{\mu_c}\right)^{0.8} \left(\frac{C_{pc}\mu_c}{k_c}\right)^{0.5} \left(\frac{\rho_w}{\rho_c}\right)^{0.3} \tag{15}$$

$$\frac{h_h D_{se}}{k_h} = 0.023 \left(\frac{\rho_c v_h D'_{se}}{\mu_h}\right)^{0.8} \left(\frac{C_{ph}\mu_h}{k_h}\right)^{0.5} \left(\frac{\rho_w}{\rho_h}\right)^{0.3} \tag{16}$$

$$\frac{h'_h D_{si}}{k_h} = 0.023 \left(\frac{\rho_c v_h D'_{se}}{\mu_h}\right)^{0.8} \left(\frac{C_{ph}\mu_h}{k_h}\right)^{0.5} \left(\frac{\rho_w}{\rho_h}\right)^{0.3} \tag{17}$$

In (18) to (20), μ, C_p and k denote viscosity, specific heat and heat conductivity of the hot and cold fluids, while D_{se} and D'_{se} are given in Eq. (18) and (19), which are the hydraulic diameters of the shell side defined as 4 × free flow area / wetted perimeter (Jiang et al., 2017).

$$D_{se} = \frac{4\left(\sqrt{3}{P_t}^2/4 - \pi {D_{to}}^2/8\right)}{\pi D_{to}/2} \tag{18}$$

$$D'_{se} = \frac{4\left(\sqrt{3}{P_t}^2/4 - \pi {D_{to}}^2/8\right)}{(\pi D_{to} + \pi D_{si}/N_t)/2} \tag{19}$$

3. Results and discussion

In this study, the HT and LT microtube recuperators are simulated using the dynamic model described in Section 2 for a pilot-scale 10 MWe sCO_2 RCBC plant. In section 3.1, the results generated by the partial differential equation (PDE) based dynamic model, setting the ACM run mode to steady state, are compared with the optimal design model using a system of algebraic equations (Jiang et al., 2017). In Section 3.2, sensitivity studies are conducted for the sizes of grids. In Section 3.3, dynamic behavior of the recuperators are studied by introducing ramp changes in the hot stream inlet temperature, where different integral step sizes are tested. In Section 3.4 and 3.5, time constants and dynamic behavior of the HT and LT recuperators are investigated by introducing step changes and fast or slow ramps to the inlet temperature and flowrate of both hot and cold fluids.

3.1 Steady-state performance and model comparison

In this section, the results generated by the PDE-based dynamic model using steady-state run mode are compared with those generated by the algebraic optimal design model developed in our previous study (Jiang et al., 2017). For each case, the axial direction is discretized into 100 grids. Table 3 shows the comparison in the heat duty, pressure drop and stream outlet conditions, while Figures 1 and 2 give the comparison in fluid and tube wall temperature profiles of the HT and LT recuperator. The temperature profiles are overlapped with each other. No significant difference is observed from the model comparison, which indicates that the PDE based model can properly predict the performance of the recuperators at steady state, while as expected the heat conduction in the shell wall does not have a strong effect on the steady-state thermal behavior of the recuperators. As shown in Figure 2, the tube wall temperature profiles almost lie in the middle of the hot and cold fluid temperature profiles for both LT and HT recuperators. This trend indicates that the heat transfer resistance of the tube and shell sides are similar, which is expected from an optimal designed heat exchanger with similar fluids in both sides.

In the design model, heat transfer in the shell wall is not considered. Hence, the steady-state results of the dynamic model are compared with or without the 1D heat conduction equation for the shell wall (w/o shell or 1D shell). The shell wall temperature profiles are plotted in Figure 3 with the hot fluid temperature profiles. Note that the shell wall temperature profile overlaps the hot side temperature profile, except at the two ends, mainly because of the no flux boundary condition, Eq. (9). A similar trend would be found in the tube wall temperature profile if zooming in on the ends in Figure 2; however, it is negligible in the tube wall because the heat flux between the tube wall and hot fluid is much larger than that between the shell wall and hot fluid, which weakens the effect of heat conduction in the tube wall.

Table 3 Comparison between the dynamic model and design model at steady-state

	HT Recuperator			LT Recuperator		
	Design	w/o shell	1D shell	Design	w/o shell	1D shell
Duty (MW)	45.15	45.19	45.19	14.48	14.52	14.52
$T_{c,out}$ (ºC)	532.07	532.13	532.13	181.95	182.42	182.42
$T_{h,out}$ (ºC)	192.95	191.28	191.28	78.20	77.90	77.90
ΔP_c (bar)	1.40	1.40	1.40	1.41	1.41	1.41
ΔP_h (bar)	1.05	1.04	1.04	1.40	1.40	1.40

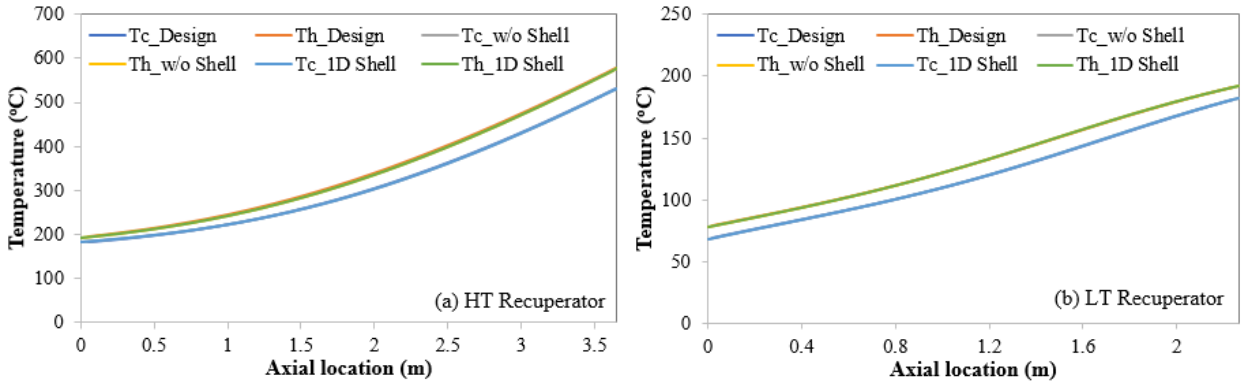

Figure 1 Model comparison in fluid temperature profiles at steady-state

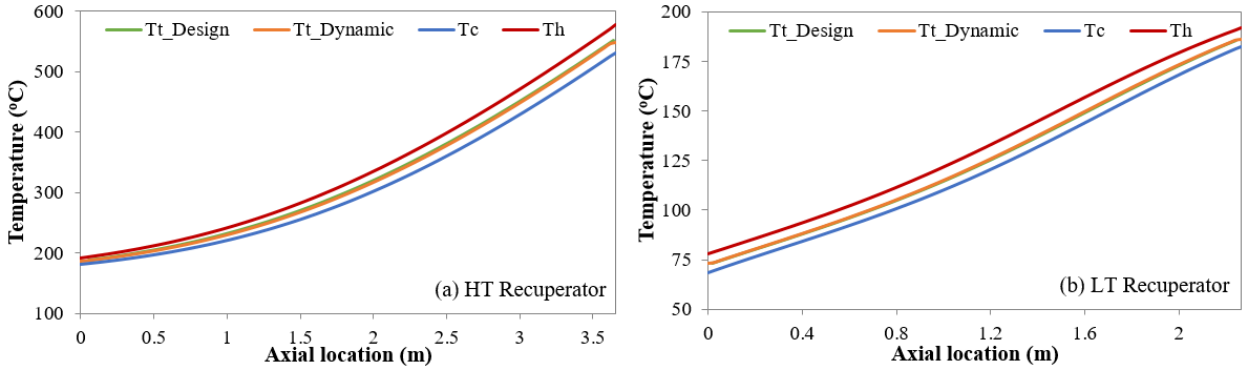

Figure 2 Model comparison in tube wall temperature profiles at steady-state

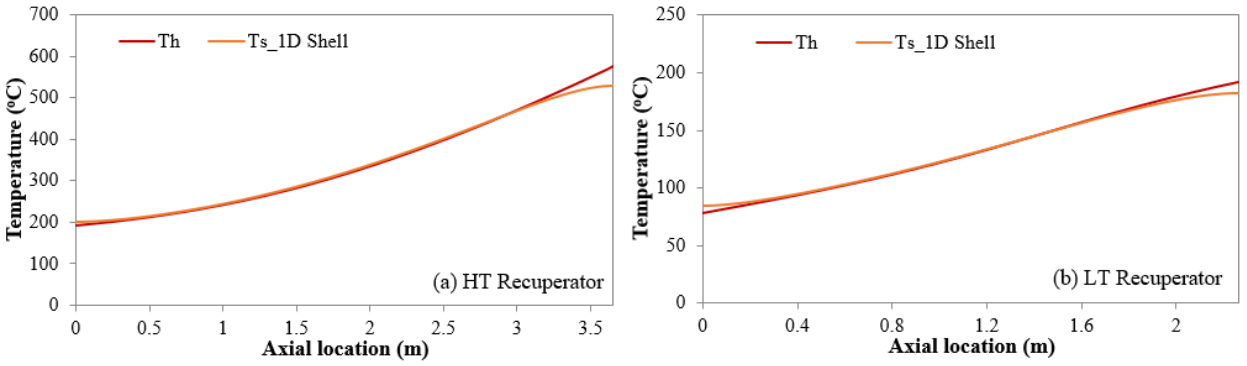

Figure 3 Model comparison in shell wall temperature profiles at steady-state

3.2 Grid sensitivity

In this section, the effect of the discretization size in the axial direction is investigated. In Figure 4, the relative error in terms of the total heat duty is plotted versus the number of grids. When the tolerance is about 0.001, it is observed that 100 and 70 grids are required for the HT and LT recuperators, respectively. This result is different from the design model (Jiang et al., 2017), since for the design model the axial direction is discretized to get the same heat duty (to improve numerical convergence) instead of the same length in each grid. In the following sections, the discretization number is set to 100 and 70 for the HT and LT recuperator, respectively.

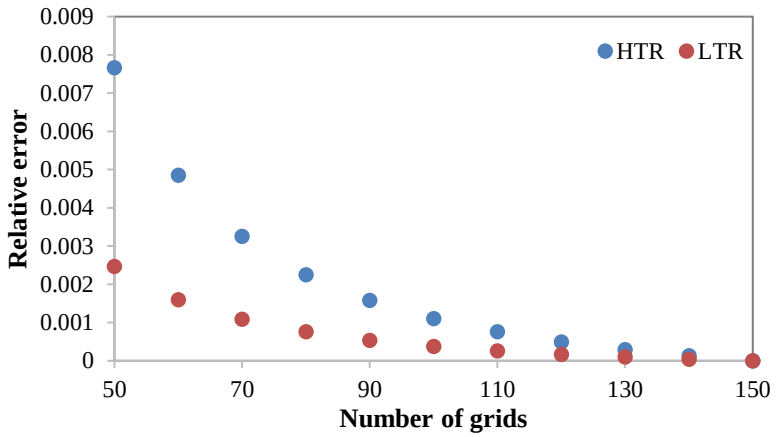

Figure 4 Grid sensitivity at steady-state

3.3 Effect of shell wall models and integral time steps on dynamic results

In this section, the effects of the shell wall models (w/o or 1D Shell) and the size of integral time steps on the dynamic simulation results of the recuperators are studied. It is noted that the size of integral time steps is in proportion to the communication time and the dimensionless step size in ACM. A 30 ^{o}C decrease in the hot side inlet temperature is introduced to HT and LT recuperators with a ramp rate of either 1 ^{o}C per sec or 1 ^{o}C per min. The axial direction is discretized into 100 grids for the HT recuperator and 70 grids for the LT recuperator. Model specification and computational time (over a 100 second or 100 minute simulation span) for five dynamic runs with the HT recuperator (1 to 5) and the LT recuperator (6 to 10) are is listed in Table 4. The cold stream outlet temperature and the hot stream inlet temperature are plotted in Figures 5 and 6 for the HT and LT recuperators, respectively. The results indicate the shell wall model has negligible effect on either the dynamic behavior of the recuperators or the computational time. In addition, the computational time can be significantly saved without affecting the results and creating numerical instability by increasing the communication time in ACM up to 1 time unit used in the model (AspenTech, 2017). For example, if the dynamic model is written with a time unit of second, then the communication time can be increased to about 1 second for less computational time.

Table 4 Model specification and computational time

Run	Shell wall	Communication Time	Computational Time
1, 6*	No	0.01 sec, 0.01 min	11 min
2, 7*	1D	0.01 sec, 0.01 min	11 min
3, 8*	1D	0.1 sec, 0.1 min	2-3 min
4, 9*	1D	0.5 sec, 0.5 min	1-2 min
5, 10*	1D	1 sec, 1 min	< 1 min

*Time unit in the heat, mass and momentum balance equations is converted to min from sec by a factor of 60

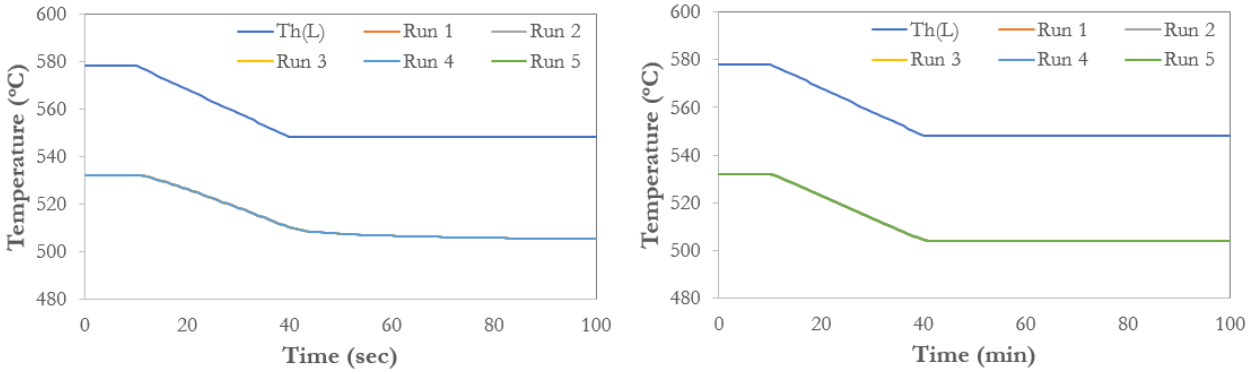

Figure 5 Dynamic behavior of the HT recuperator

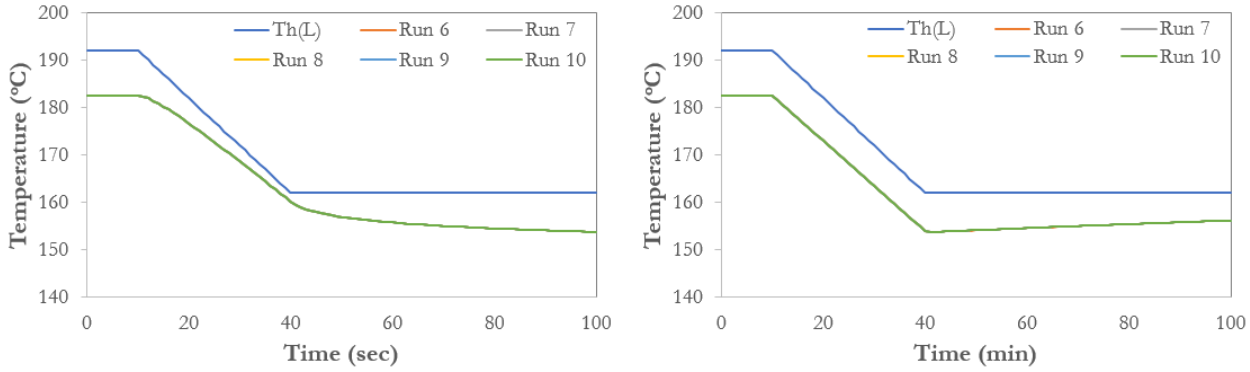

Figure 6 Dynamic behavior of the LT recuperator

3.4 Time constant of the recuperators

In this section, the time constants of the HT and LT recuperators are evaluated by introducing step changes of $\pm$ 30°C to the inlet temperature and step changes of $\pm$ 10% to the inlet flowrate of both the hot and cold fluid, as shown in Figures 7-10. Here, the time constant is a parameter characterizing the response to a step change input of a first-order time-invariant system, defined as the time for the system's step response to reach $1 - 1/e \approx 63.2\,\%$ of its final value. The values of the time constants of both recuperators are reported in Table 5. As shown in Table 5, the time constants vary from 4 sec to about 1 min, which indicates fast dynamic response of the recuperators as expected, since the optimal recuperator design gives small Biot number and larger heat transfer coefficient (Jiang et al., 2017). It is noted that the dynamic response to the step changes in temperature is faster than that in flowrate. It may because of the varying thermal holdups of the compressible fluids, and the significant changes in the heat transfer coefficients, which are highly related to Reynolds number (Jiang et al., 2017).

Table 5 Time constants of the HT and LT recuperators

	HT Recuperator				LT Recuperator			
τ (s)	$T_{c,in}$	$T_{h,in}$	$G_{c,in}$	$G_{h,in}$	$T_{c,in}$	$T_{h,in}$	$G_{c,in}$	$G_{h,in}$
$T_{c,out}$		4	40	42		6	46	50
$T_{h,out}$	10		68	63	9		43	52

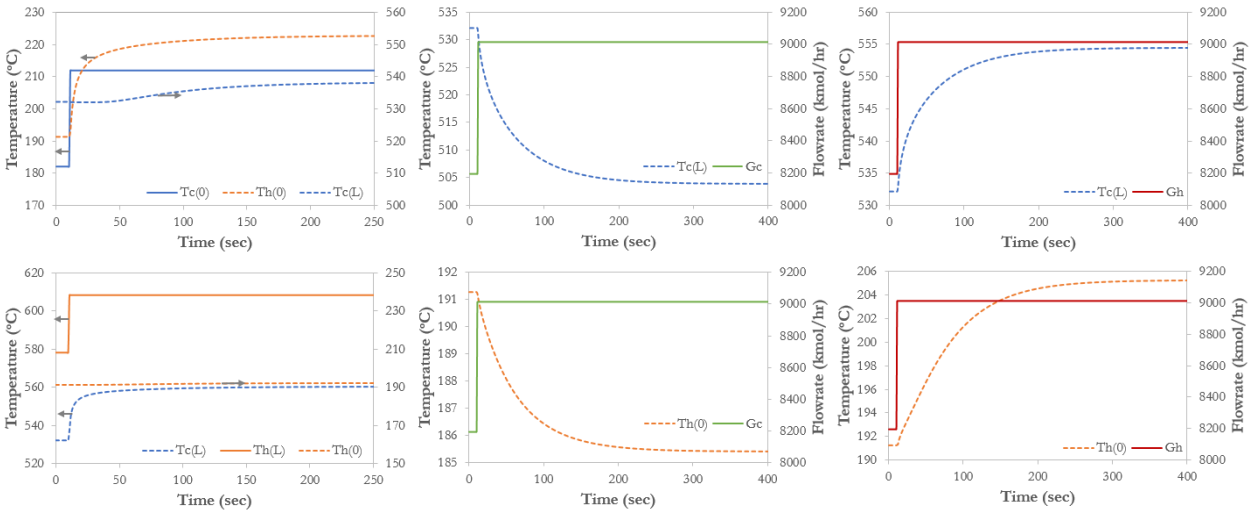

Figure 7 Step increase in the inlet temperature and flowrate of the HT recuperator

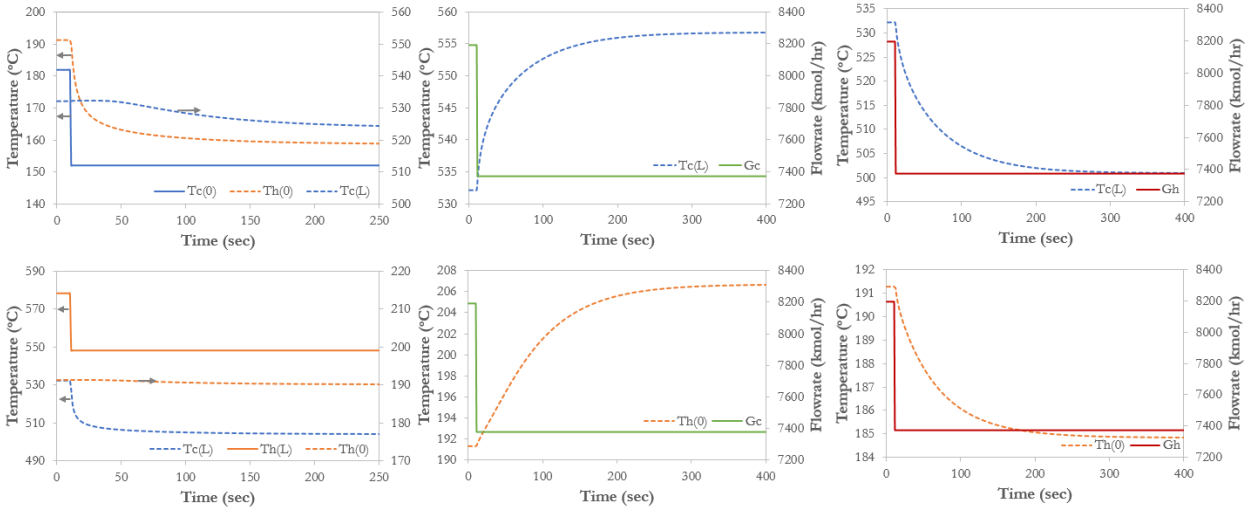

Figure 8 Step decrease in the inlet temperature and flowrate of the HT recuperator

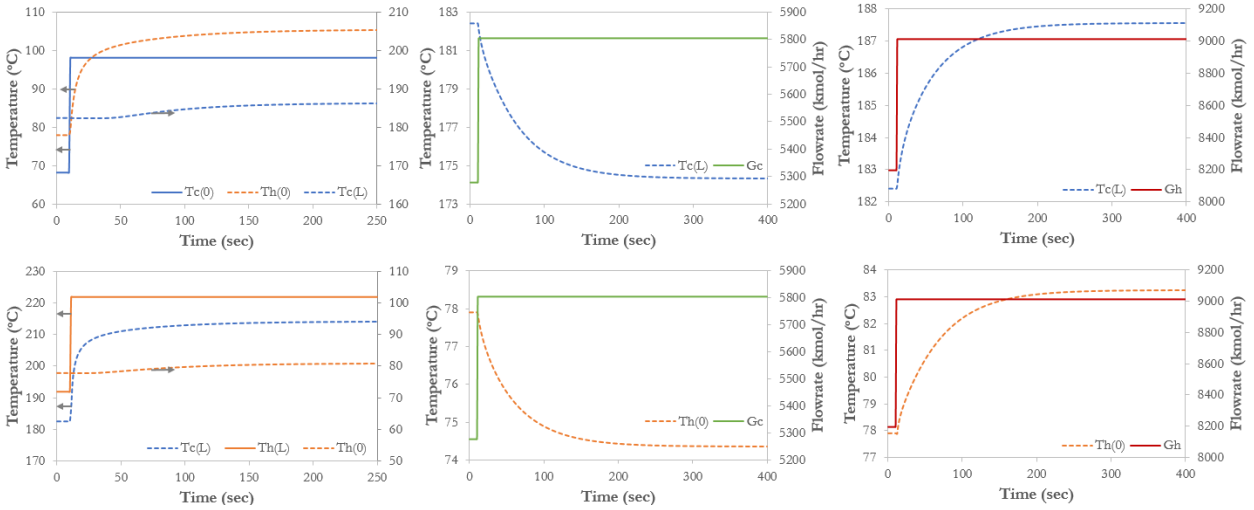

Figure 9 Step increase in the inlet temperature and flowrate of the LT recuperator

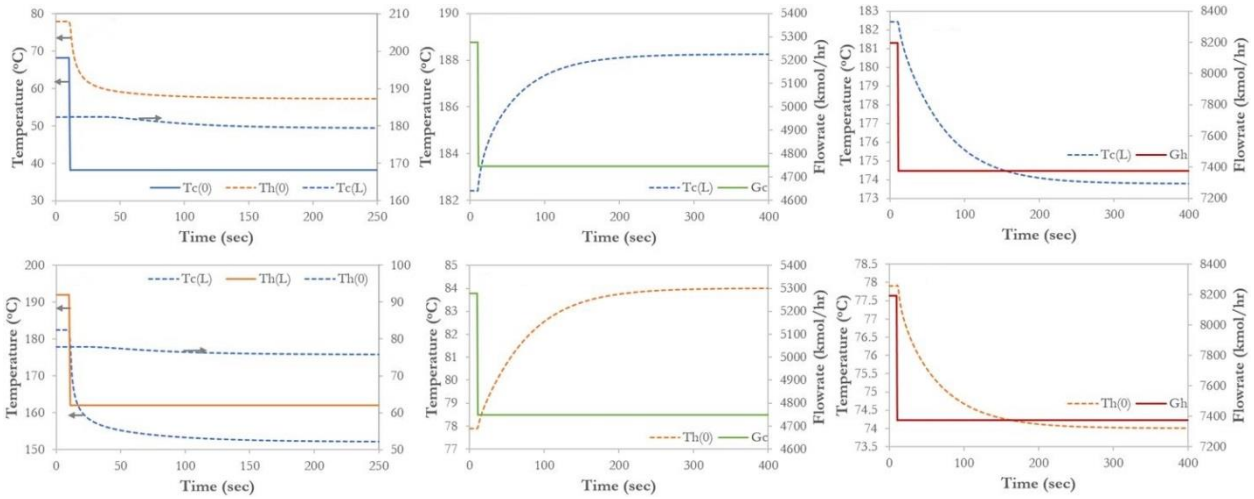

Figure 10 Step decrease in the inlet temperature and flowrate of the LT recuperator

3.4 Recuperator dynamics

In this section, the dynamic behavior is studied for the HT and LT recuperators with different ramp rates. The results are shown in Figures 11 and 13 for fast ramp rates (ramp period is per second, e.g. 30 °C for 30 seconds), and Figures 12 and 14 for slow ramp rates (ramp period is per minute). In Run 1, the dynamic profiles of the hot fluid inlet temperature (Th (L)) and cold fluid outlet temperature (Tc (L)) are plotted, when ramps in the hot fluid inlet temperature are introduced with a magnitude of $\pm$ 30 °C. In Run 2, the dynamic profiles of the cold fluid inlet temperature (Tc (0)) and the hot fluid outlet temperature (Th (0)) are plotted, when ramps in the cold fluid inlet temperature are introduced with as magnitude of $\pm$ 30 °C; In Run 3, the dynamic profiles of the cold fluid flowrate (Gc), Tc (L) and Th (0) are plotted, when ramps in the cold fluid flowrate are introduced with a magnitude of $\pm$ 10 %. In Run 4, the dynamic profiles of the hot fluid flowrate (Gh), Tc (L) and Th (0) are plotted, when ramps in the hot fluid flowrate are introduced with a magnitude of $\pm$ 10 %. As shown in Figures 8 to 10, the dynamic responses to the changes in temperature and flowrate are relatively fast, and thus the results corroborate the expectations for a very low Biot number heat exchange characteristic of compact heat exchanger design and high heat transfer coefficient of the microtube heat exchanger, in this case.

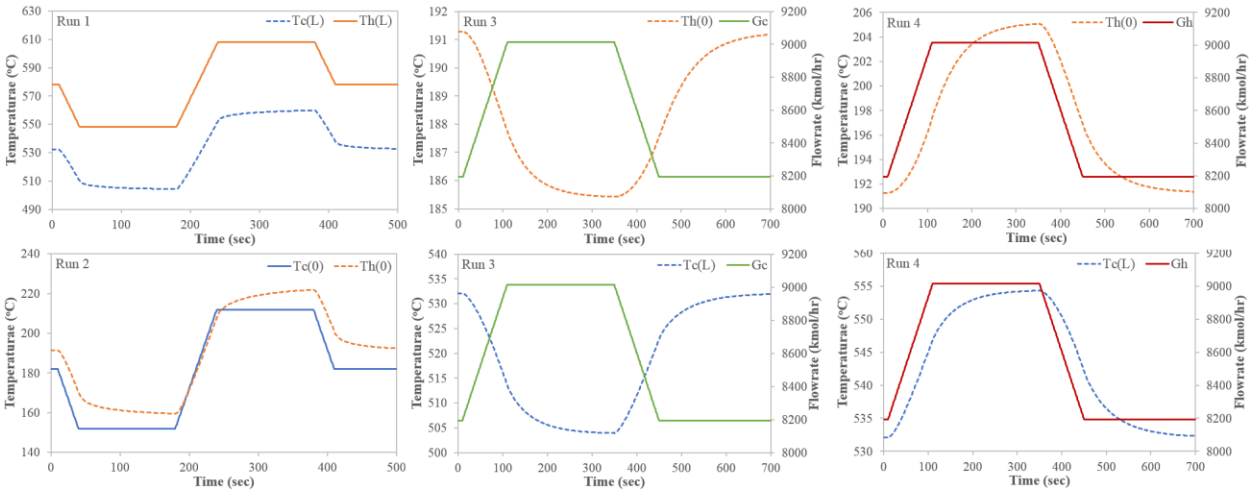

Figure 11 Dynamic behaviors of the HT recuperator with fast ramps

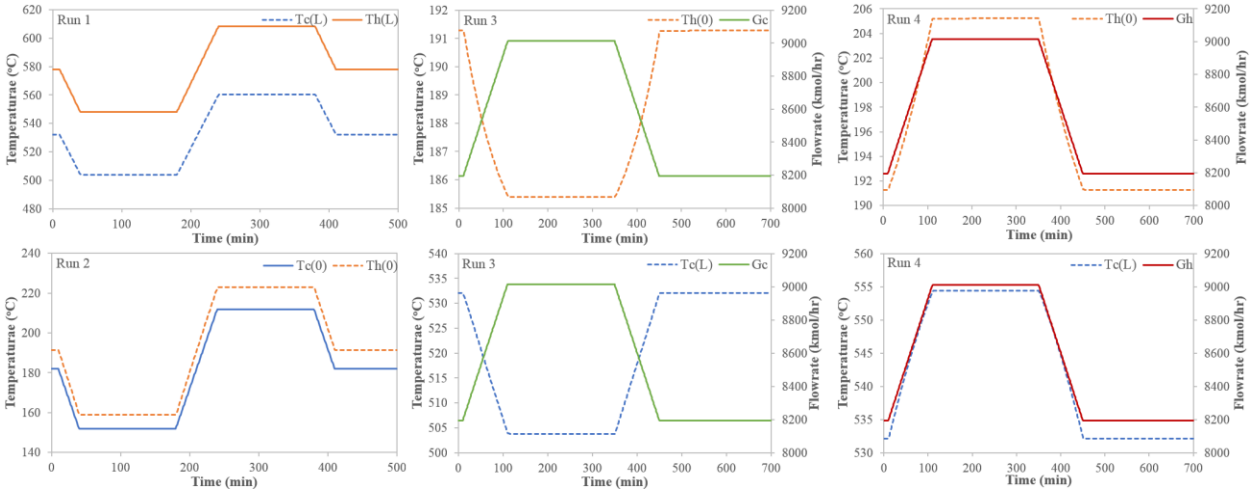

Figure 12 Dynamic behaviors of the HT recuperator with slow ramps

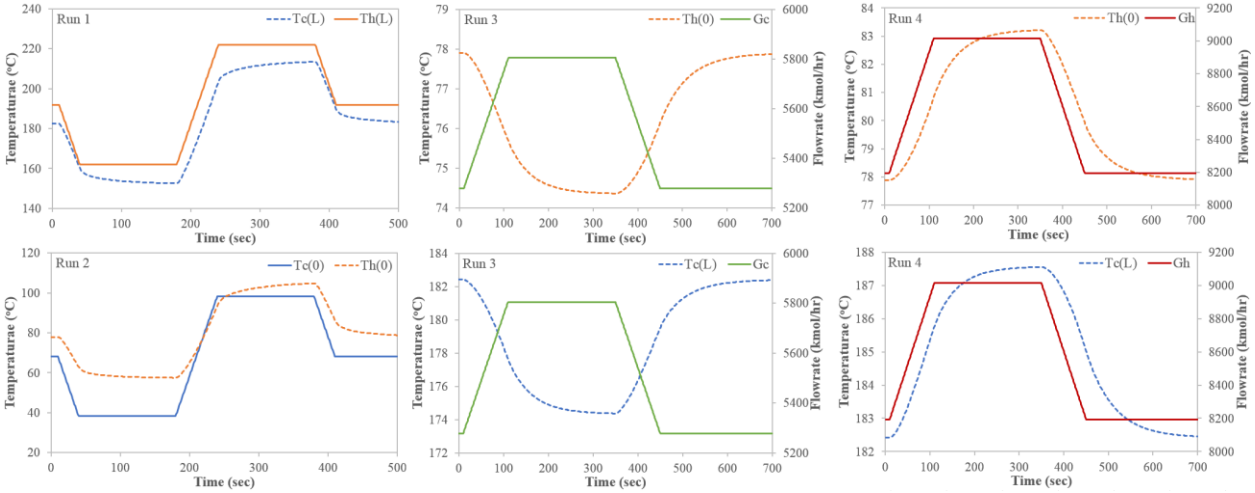

Figure 13 Dynamic behaviors of the LT recuperator with fast ramps

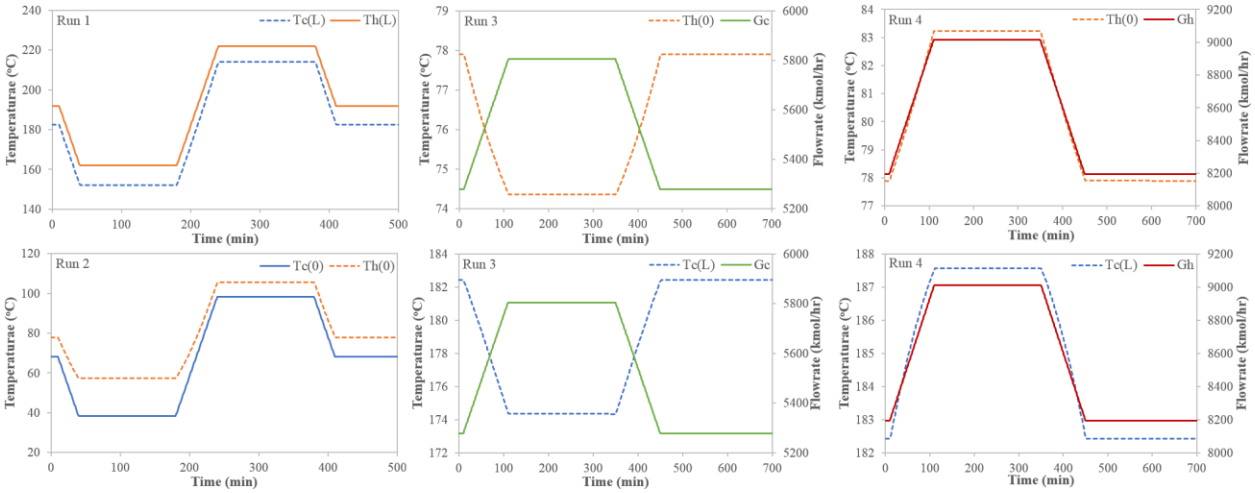

Figure 14 Dynamic behaviors of the LT recuperator with slow ramps

4. Conclusions

This paper presents a dynamic model developed in ACM for the HT and LT recuperators in a 10 MWe sCO_2 RCBC plant, of which the inlet conditions are given by the system-level studies; the geometry design is provided by the steady-state optimal design model; the heat transfer coefficients and friction factors are calculated using empirical equations proven for sCO_2 fluids. Rigorous 1D heat, mass and momentum balance equations are used to predict the temperature, velocity and pressure profiles for compressible flows. The dynamic model gives the same results as an optimal design model (Jiang et al., 2017) when running under the steady-state mode, while the heat conduction in the shell wall does not significantly affect the temperature profiles of both cold and hot fluids. Grid sensitivity shows that at least 100 and 70 grids are required for the HT and LT recuperators, respectively, to have a reasonable error tolerance. The time constants of the HT and LT are less than 10 sec if step changes are introduced to the sCO_2 inlet temperature, while they are about 1 min if step changes are introduced to the sCO_2 inlet flowrate. The dynamic responses are fast because of the small recuperator size, Biot number and the large heat transfer coefficient.

Acknowledgements

This project was supported in part by an appointment to the Science Education Programs at National Energy Technology Laboratory (NETL), administered by ORAU through the U.S. Department of Energy Oak Ridge Institute for Science and Education**.**

References

1) Zitney SE, Liese EA. Design and operation of a 10 MWe supercritical CO_2 recompression Brayton power cycle, Proceeding: Annual AIChE Meeting, San Francisco, CA, November 13-18, 2016.
2) Jiang Y, Liese E, Zitney SE, Bhattacharyya D, Optimal design of microtube recuperators in an indirect carbon dioxide recompression Brayton power cycle, submitted to Applied Thermal Engineering, 2017.
3) Jackson JD, Fluid flow and convective heat transfer to fluids at supercritical pressure, Nuclear Engineering and Design 264 (2013) 24-40.
4) Musgrove G, Sullivan S, Shiferaw D, Fourspring P, Heat exchanger, Ed, Brun K, Friedman P, Dennis R, Fundamentals and applications of supercritical carbon dioxide (sCO_2) based power cycles, Elsevier, 2017.
5) Vaitekunas DA, A Generic Dynamic Model for Crossflow Heat Exchangers with One Fluid Mixed, Thesis, McGill University, Montreal, Canada, 1990.
6) Simoes PC, Fernandes J, Paulo Mota J, Dynamic model of a supercritical carbon dioxide heat exchanger, J. of Supercritical Fluids, 35 (2005) 167-173.
7) AspenTech, http://www.aspentech.com/products/engineering/aspen-custom-modeler/, accessed on April 2017.
8) NETL, Recuperator Technology Development and Assessment for Supercritical Carbon Dioxide (SCO2) Based Power Cycles, Funding Opportunity Number: DE-FOA-0001239, March 2015.
9) Guo J, Design analysis of supercritical carbon dioxide recuperator, Applied Energy 164 (2016) 21-27.
10) Xie GN, Sunden B, Wang QW, Optimization of compact heat exchangers by a genetic algorithm, Applied Thermal Engineering, 28 (2008) 895-906.
11) Schmitt J, Amos D, Kapat J, Design and real fluid modelling of micro-channel recuperators for a nominal 100MW class recuperated recompression Brayton cycle using supercritical carbon dioxide, GT2015-43761, Proceedings of ASME Turbo Expo 2015: Turbine Technical Conference and Exposition, June 15-19, 2015, Montreal, Canada.
12) Carstens NA, Control Strategies for Supercritical Carbon Dioxide Power Conversion Systems, Doctor Dissertation, Massachusetts Institute of Technology, Cambridge, MA, 2007.
13) Kruizenga A, Fleming D, Carlson M, Anstey M, Supercritical CO_2 heat exchanger fouling, in Proceedings: the 4th International Symposium – Supercritical CO_2 Power Cycles, September 9-10, 2014, Pittsburgh, Pennsylvania.
14) Francesco C, Piero C, Development of a Modelica dynamic model of solar supercritical CO_2 Brayton cycle power plants for control studies, in Proceedings of Supercritical CO_2 Power Cycle Symposium, May 24-25, 2011, Boulder, Colorado.

15) Luu MT, Milani D, McNaughton R, Abbas A, Dynamic modelling and start-up operation of a solar-assisted recompression supercritical CO_2 Brayton power cycle, Applied Energy, 199 (2017) 247-263.
16) Ahn Y, Bae SJ, Kim M, Cho SK, Baik S, Lee JI, Cha JE, Review of supercritical CO_2 power cycle technology and current status of research and development, Nucl. Eng. Technol. 24 (2015) 647-661.
17) Chordia L, Green E, Li D, Portnoff M, Development of modular, low-cost, high-temperature recuperators for the sCO_2 power cycles, NETL 2016 University Turbine Systems Research Project Review Meeting, Blacksburg, VA, 2016.
18) Span R, Wagner W, A new equation of state for carbon dioxide covering the fluid region from the triple-point temperature to 1100 K at Pressures up to 800 MPa, J. Phys. Chem. Ref. Data, Vole. 25 No.9, 1996.